IMPROVED METHODS FOR CALCULATING THE THICKNESS NOISE

Yoshiya Nakamura and Akira Azuma
University of Tokyo

SUMMARY

Three advanced methods to compute the rotor thickness noise which is predominant in the case of high speed rotor have been developed. These methods are deduced from a previous method by transforming the integral coordinate, commuting the order of integration and differentiation, and/or performing chordwise integration analytically with some adequate assumptions. The necessary computational times and waveforms obtained by the previous and three advanced methods were compared. It was then concluded that the advanced methods could save the computational time very much compared with the previous method in keeping the same accuracy.

INTRODUCTION

Farassat has proposed a method to calculate the thickness noise which is produced by moving bodies of finite volume or thickness normal to the moving direction and applied it to the rotor noise of helicopters (ref.1).

Based on his work, the authors made clear the cause and the characteristics of the rotor rotational noise. Through these studies (ref.2 and 3) with the concept of the "influential surface", which is an integral region at retarded time, and of the distribution of source strength, many acoustic characteristics of helicopter rotor noise have been clarified by the analytical predictions and numerical calculations, and verified by the experimental tests. It has been shown that among the rotor rotational noise components the rotor thickness effect executes a dominant roll rather than the loading effects such as thrust noise and drag noise in the case of high blade-tip speed.

In the computational process of the thickness noise, however, the calculation has the worst converging characteristics and thus needs a lot of computer time in getting solutions within enough accuracy. It has, therefore, been expected to develop an improved method of calculation for obtaining an advanced form of solution which is more convenient to get the result with less computer time and enough accuracy.

SYMBOLS

B	number of blades
c_0	sound speed, m/sec
C_h	chord length
$f=0$	equation of body surface
	$= \begin{cases} \eta_3-h(\eta_1, \eta_2) & \text{at the upper surface} \\ -\eta_3-h(\eta_1, \eta_2) & \text{at the lower surface} \end{cases}$
$g=0$	equation of acoustic sphere $= \tau-t+[r]_{ret}/c_0$
h	blade thickness, m
K	integrand of a modified solution of thickness noise, see equation (10)
M_r	relative Mach number
p	acoustic pressure, kg/m^2
R	rotor radius, m
R_0	blade cut-off radius, m
r	distance between source and observer, $=\|x-y\|$, m
r_0	distance between hub center and observer, m
$\hat{r}_\eta$	unit vector in direction of propagation in blade fixed coordinate
	$\begin{cases} =(\hat{r}_{\eta_1}, \hat{r}_{\eta_2}, \hat{r}_{\eta_3})^T = (\partial r/\partial\eta_1, \partial r/\partial\eta_2, \partial r/\partial\eta_3)^T \\ =(\dfrac{r_1\sin\psi-r_2\cos\psi}{r}, 0, \dfrac{r_3}{r})^T \end{cases}$
t	observer time
V	rotor hub velocity, $=(V_1, V_2, V_3)^T$, m/sec
V_η	$=(V_{\eta_1}, V_{\eta_2}, V_{\eta_3})^T$, m/sec
v_n	blade element velocity normal to blade surface, m/sec
x	observer position vector, $=(x_1, x_2, x_3)^T$, m
y	source position vector, $=(y_1, y_2, y_3)^T$, m

α angle between radiating direction and rotor plane, rad or deg

Γ curve of intersection of body with acoustic sphere

η position vector in blade fixed Cartesian coordinate system

θ angle between radiating direction and normal direction to blade surface, rad or deg

ρ density of undisturbed fluid, $kg \cdot sec/m^4$

τ source time, sec

ψ blade azimuth angle, rad or deg

Ω rotor rotational speed, rad/sec

Λ directional parameter in modified method, see equation (8)

λ directional parameter in previous method, see equation (3)

Superscript

$( )^T$ transposed of ( )

Subscript

$[ ]_{ret}$ value at a retarded time

Operator

∇ gradient operator in fluid fixed coordinate, $=\partial/\partial y_i$, 1/m

PREVIOUS ANALYSIS — METHOD (A)

According to Farassat (ref.1), the rotor thickness noise, p, for a given observer position, x, and time, t, is given by

$$p(x,t) = \frac{\rho c_0}{2\pi} \frac{\partial}{\partial t} \int_{\tau_1}^{\tau_2} \int_{\Gamma} \frac{(\partial h/\partial \eta_1) V_{\eta_1}}{r\lambda} d\Gamma d\tau \qquad (1)$$

where $h(\eta_1)$ is the blade thickness distribution as a function of chordwise coordinate, η_1. Here the relative speed of a blade element with respect to the fluid and the directional parameter, λ, are respectively given by

$$V_{\eta_1} = V_1 \sin\psi - V_2 \cos\psi + \eta_2 \Omega, \qquad (2)$$

$$\lambda = |\nabla f|\sin\theta = |(-\partial h/\partial\eta_1,\ -\partial h/\partial\eta_2,\ \pm 1)^T|\sin\theta$$
$$= \{1-\hat{r}^2_{\eta_3} + (\partial h/\partial\eta_1)^2(1-\hat{r}^2_{\eta_1})\}^{1/2}, \tag{3}$$

where r is the distance between the observer and the source, and ∇f means the vector outward normal to the blade surface. Other symbols related to the above equations are listed in SYMBOLS.

The integrations appearing in equation (1) may be understood as follows: In order to calculate the noise field of a moving source, the concept of retarded time designated by $[\ ]_{ret}$ must be considered, because the pressure change generated at different points and times might be received by an observer at a given time simultaneously. It is, thus, useful to know all regions of noise sources that have influence on the observer at the given time. These regions will be formed by the loci or trajectories of closed curves called "Γ-curves" for the given observer time and position with the change of the source time, $-\infty<\tau\leq t$.

An external surface of each region has been named "influential surface". All sources distributed on these surfaces must be integrated to give the instantaneous pressure of the given observer time and position. By considering the shape of the respective influential surface, many typical effects of various rotor operating parameters on each noise component have come to be predictable analytically (ref.2 and 3).

The integration $\int_{\tau_1}^{\tau_2}\int_{\Gamma} d\Gamma c_0 d\tau$ should be performed on the influential surfaces which are the loci of intersections between an "acoustic sphere," $g=t-\tau-[r]_{ret}/c_0=0$, and blade surfaces, $f(y,\tau)=0$, for a given observer time, t. The times specified by τ_1 and τ_2 are source times at which the acoustic sphere enters and leaves the blade respectively. With the lapse of the source time, the acoustic sphere contracts toward its center, just where the observer locates, with the speed of sound, c_0, while the blade rotates around the rotor axis. Fig.1 shows the geometric arrangements of an influential point. The influential point is given as the intersection between an acoustic line and a specified point, (η_1,η_2), on the i-th blade and is determined by the following equation:

$$F \equiv \cos\alpha\cdot(\eta_2\cos\psi-R)\Omega/c_0+\psi$$
$$-(\Omega t+2\pi(i-1)/B-\eta_1/\eta_2) = 0, \tag{4}$$

where

$$0\leq\eta_1\leq C_h$$
$$R_0\leq\eta_2\leq R. \tag{5}$$

The angular velocity of the influential point, $\partial\psi/\partial t$, which plays an important role in the noise calculation as will be stated later, can be derived by differentiating equation (4) as

$$\partial\psi/\partial t = \Omega/(1-M_r), \tag{6}$$

where M_r is relative Mach number of the specified blade position with respect to an observer. Since M_r has positive peak at $\psi=90°$, $\partial\psi/\partial t$ takes maximum value at this azimuthal position.

In the numerical calculation by the previous method, factors which decide the precision level of calculation are: i) mesh dimension of the Simpson sum, ii) dimension of the observer time increment, iii) precision rank adopted in the computation. After some trial computations by using a computer, FACOM 230/75, it was concluded that the double precision was necessary and sufficient for the present calculation and that the number of integrating point for obtaining reliable results was about 10^4, which corresponded to the following dimension for one element: The tangential partition was (chord length)/20; the radial partition was (rotor radius)/300; and $\Delta\eta=0.16$. This mesh dimension required about twenty seconds to compute the total pressure value of a given observer time and position. Then it was decided that the number of discrete observer times in the one blade passing period was thirty six in order to give a total computational time within twenty minutes.

MODIFIED ANALYSES — METHODS (B) AND (C)

Undesirable defects on the accuracy in the previous computation were caused by the numerical differentiation, $\partial/\partial t$, and the numerical double integration on the influential surfaces, $\int\int d\Gamma d\tau$. If the observer time differentiation, $\partial/\partial t$, can be put inside the integration, and be performed analytically, then the numerical differentiation will disappear and very much computational time can be saved.

In the previous analysis, the integration on the influential surface was performed along a contracting acoustic sphere, $d\Gamma d\tau$. Here, in the present analyses, by using a polar coordinate system associated with the rotor disk, an elemental area of the integration, $\eta_2 d\psi d\eta_2$, can be transformed as follows:

$$\frac{c_0 d\Gamma d\tau}{\lambda/|\nabla f|} = \frac{\eta_2 d\psi d\eta_2}{\Lambda} \tag{7}$$

where

$$\Lambda = (1+M_n^2-2M_n\cos\theta)^{1/2}$$

$$M_n = v_n/c_0 \tag{8}$$

$$v_n = -\frac{\partial f}{\partial \tau}/|\nabla f| = \frac{\partial h}{\partial \eta_1} V\eta_1/|\nabla f|.$$

Then, by using the above relation, the solution of wave equation of the rotor thickness noise can be rewritten in the new coordinate system as follows:

$$p(x,t) = \frac{\rho}{2\pi}\frac{\partial}{\partial t}\sum_{i}^{B}\int_{R_0}^{R}\left[\int_{\psi_2}^{\psi_1} K d\psi\right]_{ret} \eta_2 d\eta_2 \tag{9}$$

where

$$K = \frac{\partial h}{\partial \eta_1} V\eta_1 / r|\nabla f|\Lambda. \tag{10}$$

In the ranges of integrations, ψ_1 and ψ_2 are the azimuth angles of the leading edge and trailing edge of the influential surface respectively, which are functions of the span position, η_2, the observer time, t, and position, x; and R and R_0 are the rotor radius and the blade cut-off radius respectively. The integrand, K, is considered to be a function of independent variable, η_1 or ψ, η_2, t, and x. Thus, the double integration, $\int\int \eta_2 d\psi d\eta_2$, gives an influential-surface integration of a single blade.

Fig.2 shows two different arrangements of integrating points on the same influential surface. It can be seen that the present methods have a well-fitting coordinate converging to the integral region. The method (B) is derived from equation (9) by performing numerically the differentiation and the integration.

By commuting the order of the differentiation and the integration, equation (9) becomes

$$p(x,t) = \frac{\rho}{2\pi}\sum_{i}^{B}\int_{R_0}^{R}\left[\int_{\psi_2(t)}^{\psi_1(t)} \frac{\partial K(\psi)}{\partial t}\bigg|_{\psi,\eta_2} d\psi - K(\psi_2)\frac{\partial \psi_2}{\partial t} + K(\psi_1)\frac{\partial \psi_1}{\partial t}\right]_{ret} \eta_2 d\eta_2, \tag{11}$$

where $\partial K(\psi)/\partial t$ should be considered as follows:

$$\left.\frac{\partial K}{\partial t}\right|_{\psi,\eta_2} = \left[\left.\frac{\partial K}{\partial t}\right|_{\eta_1} + \frac{\partial K}{\partial \eta_1}\frac{\partial \eta_1}{\partial t}\right]_{\psi,\eta_2}$$

$$= \left[\frac{\partial K}{\partial r}\frac{\partial r}{\partial t} + \frac{\partial K}{\partial \Lambda}\frac{\partial \Lambda}{\partial t}\right]_{\eta_1,\eta_2,\psi} + \left[\left(\frac{\partial K}{\partial(\partial h/\partial \eta_1)}\frac{\partial^2 h}{\partial \eta_1^2}\right.\right. \tag{12}$$

$$\left.\left. + \frac{\partial K}{\partial V_{\eta_1}}\frac{\partial V\eta_1}{\partial \eta_1} + \frac{\partial K}{\partial r}\frac{\partial r}{\partial \eta_1} + \frac{\partial K}{\partial |\nabla f|}\frac{\partial |\nabla f|}{\partial \eta_1} + \frac{\partial K}{\partial \Lambda}\frac{\partial \Lambda}{\partial \eta_1}\right)\frac{\partial \eta_1}{\partial t}\right]_{\eta_2,\psi}.$$

The method (C) is derived from equation (11) by performing the numerical integration.

ANALYTIC METHOD — METHOD (D)

Consider the following case for simplicity of analysis:

(i) hovering state, $V_{\eta_1} = \eta_2\Omega$

and (13)

(ii) far field, $R \ll r$ that is $r=r_0=\text{const.}$, $\Lambda=1$, and $|\nabla f|=1$.

Then the kernel given by equation (10) and the acoustic pressure can be written respectively as follows:

$$K = (\partial h/\partial \eta_1)\eta_2\Omega/r_0 \tag{14}$$

and

$$\begin{aligned} p(x,t) &= \frac{\rho\Omega}{2\pi r_0}\int_{R_0}^{R}\eta_2^2\left[\frac{\partial}{\partial t}\int_{\psi_2}^{\psi_1}\frac{\partial h}{\partial \eta_1}d\psi\right]_{ret}d\eta_2 \\ &= \frac{\rho\Omega}{2\pi r_0}\int_{R_0}^{R}\eta_2^2\left[\int_{\psi_2}^{\psi_1}\left[\frac{\partial}{\partial t}\left(\frac{\partial h}{\partial \eta_1}\right)\right]_{\psi}d\psi+\left.\frac{\partial h}{\partial \eta_1}\right|_{\psi_1}\frac{\partial \psi_1}{\partial t}-\left.\frac{\partial h}{\partial \eta_1}\right|_{\psi_2}\frac{\partial \psi_2}{\partial t}\right]_{ret}d\eta_2 \\ &= \frac{\rho\Omega}{2\pi r_0}\int_{R_0}^{R}\eta_2^2\left[\int_{\psi_2}^{\psi_1}\left(\frac{\partial^2 h}{\partial t\partial \eta_1}+\frac{\partial^2 h}{\partial \eta_1^2}\left.\frac{\partial \eta_1}{\partial t}\right|_{\psi}\right)d\psi+\left.\frac{\partial h}{\partial \eta_1}\right|_{\psi_1}\frac{\partial \psi_1}{\partial t}-\left.\frac{\partial h}{\partial \eta_1}\right|_{\psi_2}\frac{\partial \psi_2}{\partial t}\right]_{ret}d\eta_2. \end{aligned} \tag{15}$$

In a double parabolic airfoil, for example, the thickness change can be given by

$$\frac{\partial h}{\partial \eta_1} = \frac{2h_{max}}{C_h}(1-2\eta_1/C_h), \tag{16}$$

which is, at the leading edge, $\eta_1=0$ $(\psi=\psi_1)$, and the trailing edge, $\eta_1=C_h(\psi=\psi_2)$, given by

$$\left.\frac{\partial h}{\partial \eta_1}\right|_{\psi_1} = -\left.\frac{\partial h}{\partial \eta_1}\right|_{\psi_2} = \frac{2h_{max}}{C_h}. \tag{17}$$

Combining equations (16) and (4) yields

$$\frac{\partial h}{\partial \eta_1} = \frac{2h_{max}}{C_h}\left[\,1-\frac{2\eta_2}{C_h}\left\{\Omega t+\frac{2\pi}{B}(i-1)\right.\right.$$

$$\left.\left.-\psi-\frac{\Omega}{c_0}(\eta_2\cos\psi-R)\cos\alpha\right\}\right]. \tag{18}$$

By substituting the above two relations into equation (15), the acoustic pressure can be obtained in a decomposed form as follows:

$$p(x,t) = p_1(x,t)+p_2(x,t)+p_3(x,t)$$

where

$$p_1(x,t) = \frac{\rho\Omega h_{max}}{\pi r_0 C_h}\int_{R_0}^{R}\eta_2^2\left\{-\frac{2\eta_2\Omega}{C_h}(\psi_1-\psi_2)\right\}d\eta_2$$

$$p_2(x,t) = \frac{\rho\Omega h_{max}}{\pi r_0 C_h}\int_{R_0}^{R}\eta_2^2\dot{\psi}_1 d\eta_2 \tag{19}$$

$$p_3(x,t) = \frac{\rho\Omega h_{max}}{\pi r_0 C_h}\int_{R_0}^{R}\eta_2^2\dot{\psi}_2 d\eta_2.$$

As written above, the chordwise integration and the time differentiation have been performed analitically. Three components of equation (19) are corresponding to the first, second, and third terms of equation (11) exactly. An example of computed waveform is shown in Fig.3, in which solid lines show components of the respective term and a dotted line shows the total acoustic waveform obtained by summing up these three components.

As shown in Fig.4, the influential surfaces of multi-bladed rotor can be made from those of one blade at appropriate observer time. Then, once the sound pressure of one blade is computed, the acoustic pressure of the multi-bladed rotor can be easily obtained by summing up those of each blade one after another. Fig.5 shows an example of this process for three bladed rotor.

COMPUTATIONAL RESULTS

The dimensions of an exemplified rotor are given in Table I. The computational procedure is shown in Fig.6. Shown in Fig.7 is an example of the

computed waveforms by four different methods, (A) through (D). It can be seen that these four methods give the very good coincidence in the waveform and the negative peak value, but a slight difference in the positive peak value. The difference between the waveforms of (B) and (C) is too small to be distinguished. It is interesting to note that the area made by the positive acoustic pressure and zero line in one period is equal to that made by the negative one.

Fig.8 shows the change of computed pressure amplitude in methods (B) and (C) in relation to the spanwise mesh size for a given chordwise mesh size by circles, and to the chordwise mesh size for a given spanwise mesh size by triangles. The difference of sensitivity of the accuracy for the number of spanwise and chordwise partitions are obvious. The insensitive tendency of the chordwise partition may result mostly from the blade contour of symmetric profile without singularity.

Fig.9 shows the computed pressure amplitudes or peak values of pressure versus the number of spanwise partitions in four methods. As the number of partitions increases the pressure converges to an expected true value whereas the computation time increases predominantly as shown in Fig.10. It can be seen that choice of proper coordinate, analytic chordwise integration, and the consequently simplified program used in the present methods saved the computational time significantly. This guarantees that the present methods (C) and (D) need respectively only one tenth and one hundredth of the computational time of the method (A) to get the acoustic pressure in the same accuracy.

CONCLUSION

Four different methods to compute the rotor thickness noise have been compared. They are (A) the previous method based on equation (1); (B) the one modified method based on equation (9) in which the surface integration is performed in the rotor-fixed-coordinate system; (C) the other modified method based on equation (11) in which the numerical differentiation is discarded; (D) the still other modified method based on equation (19) in which the numerical chordwise integration is further discarded. All methods have shown the good coincidence in both the waveform and the peak amplitude.

The introduction of the rotor-fixed-polar-coordinate system has brought better characteristics in convergence and accuracy of the numerical integration than the previous method (A) in which the observer-fixed-polar-coordinate system was adopted. Specifically, the method (D), in which the chordwise integration was performed analytically by assuming the hovering state of rotor and the far field location of observer, has saved further computational time. The computational time in the method (D) was only one hundredth of method (A) and one tenth of methods (B) and (C) in keeping the same accuracy. It can, thus, be concluded that the computing method of the rotor thickness noise was improved very much by introducing the advanced methods (C) and (D) in the accuracy and speed.

REFERENCES

1. Farassat, F.: Theory of Noise Generation From Moving Bodies With an Application to Helicopter Rotors, NASA TR R-451, Dec. 1975.

2. Nakamura, Y.: Helicopter Noise. PhD Thesis, University of Tokyo, March, 1977.

3. Nakamura, Y.: The Analysis of Helicopter Rotor Noise, ISAS Report No. 549 (Vol. 42, No. 4), Institute of Space and Aeronautical Science, University of Tokyo, Sept. 1977.

TABLE I

Dimensions:

Rotor radius; R, m	5.0
Blade cut off; R_0,m	0.7
No. of blades; B	2
Blade chord ; C_h, m	0.4
Blade thickness ratio; h_{max}/C_h	0.10
Airfoil section	NACA 0010

Operating conditions:

Forward speed; V, m/sec	0 (hovering)
Tip Mach number; M_t	0.9

Observer:

Observer position; r_0,m	50
Observer elevation angle;α_0,deg	0

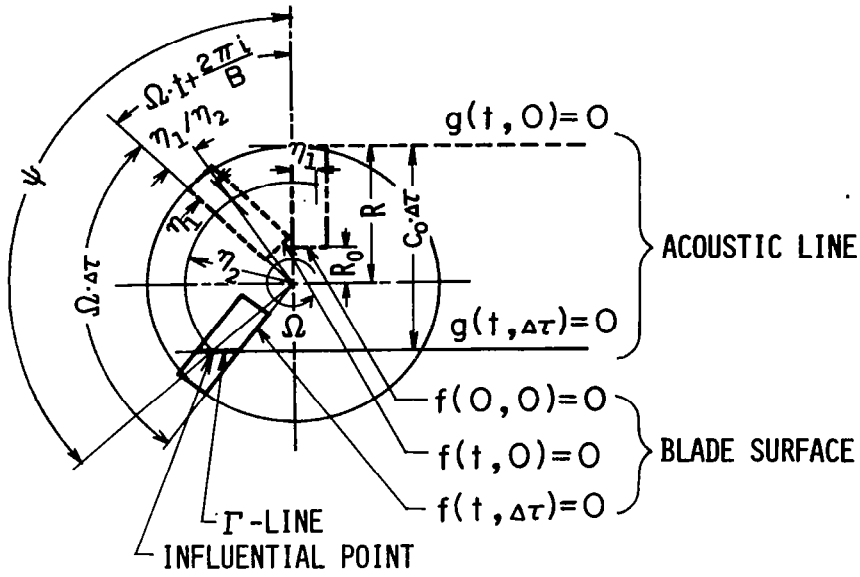

$$F=\cos\alpha(\eta_2\cos\psi-R)\Omega/c_0+\psi-(\Omega t+2\pi i/B-\eta_1/\eta_2)=0$$

Figure 1.- Geometric arrangements of an influential point.

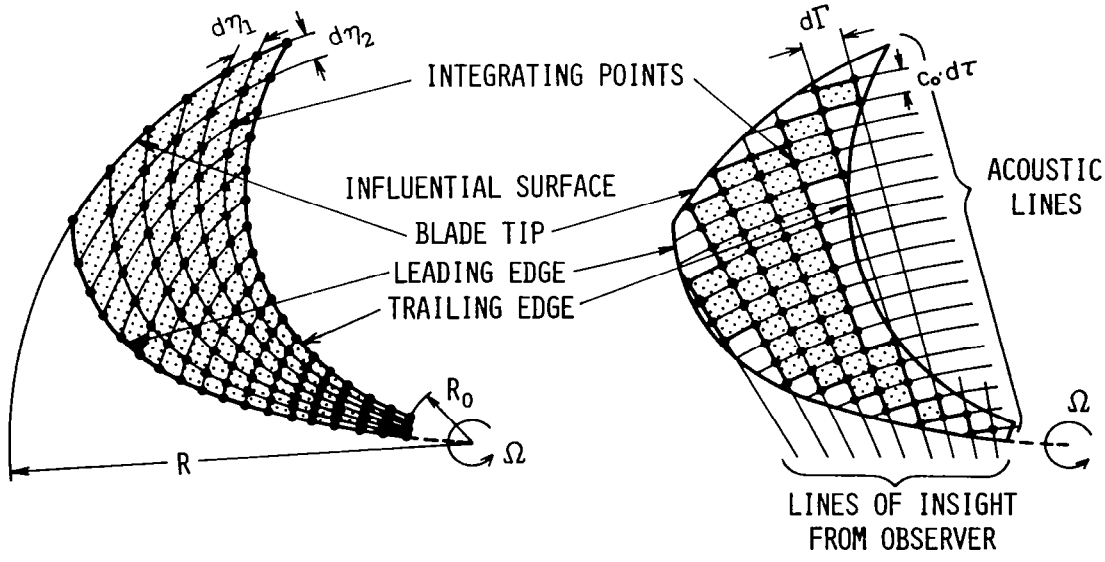

(a) Present methods. (b) Previous method.

Figure 2.- A comparison of integrating mesh between two coordinate systems

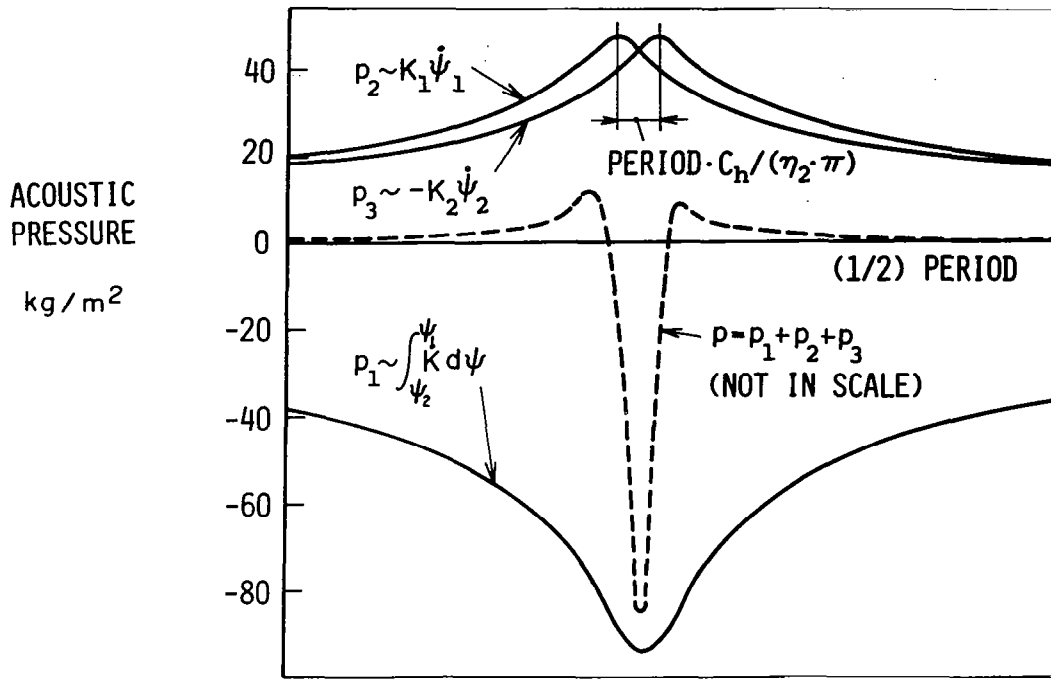

Figure 3.- Computation of waveform.

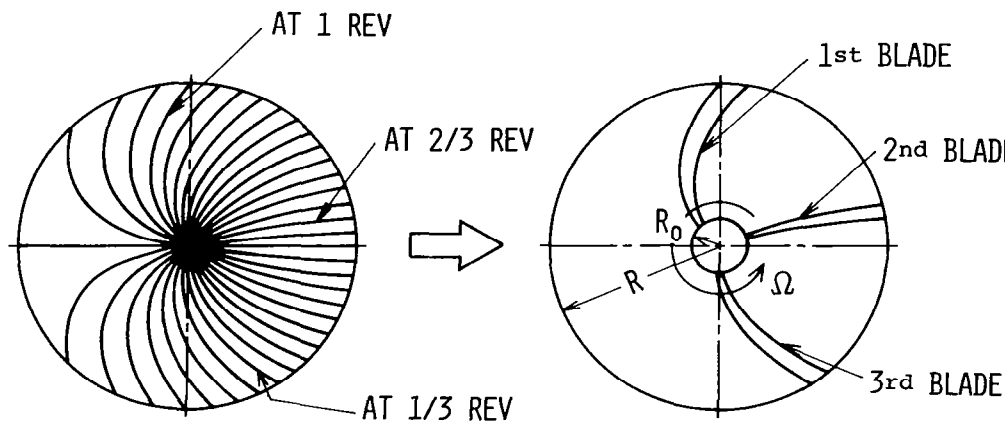

(a) Influential lines of leading edge of one blade at each observer time.

(b) Influential surfaces of three bladed rotor at given observer time.

Figure 4.- An example to obtain influential surfaces of multi-bladed rotor from influential lines.

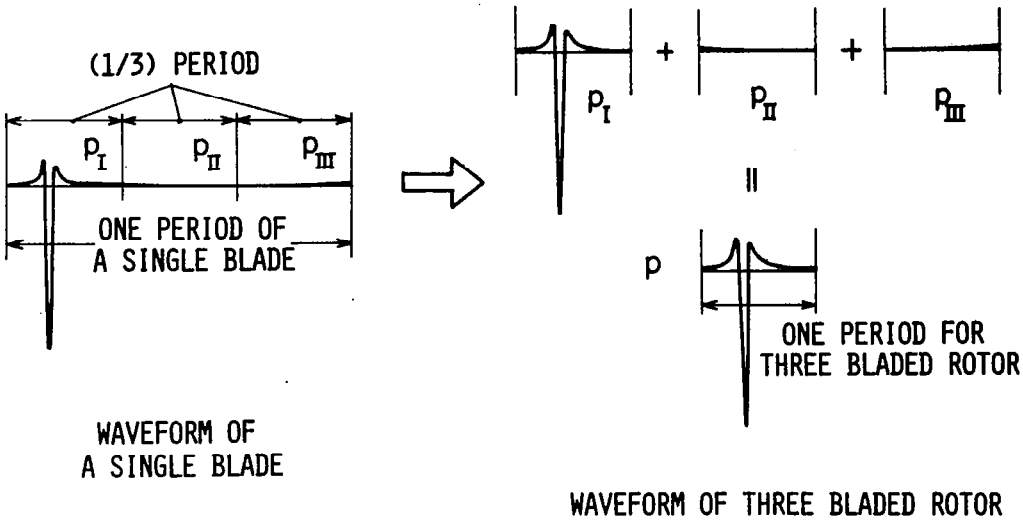

Figure 5.- An example to obtain waveform of multi-bladed rotor from a waveform of single blade.

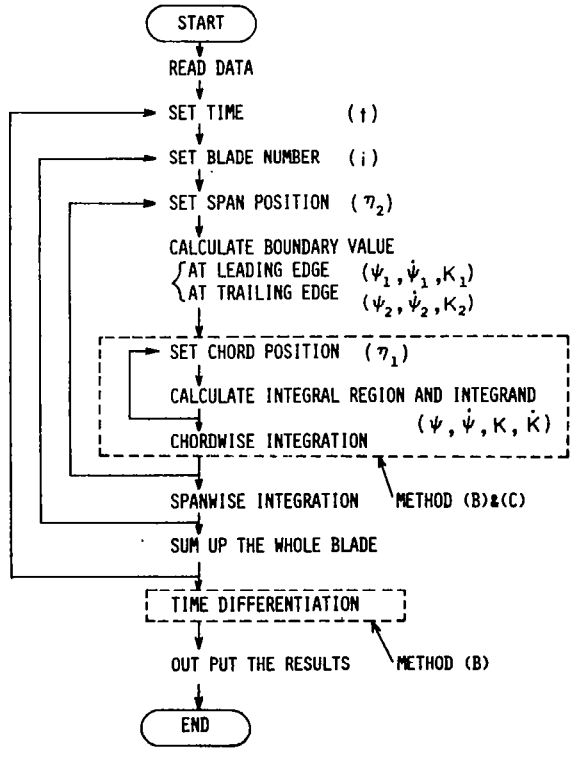

Figure 6.- Flowchart of modified mehtods to compute the rotor thickness noise.

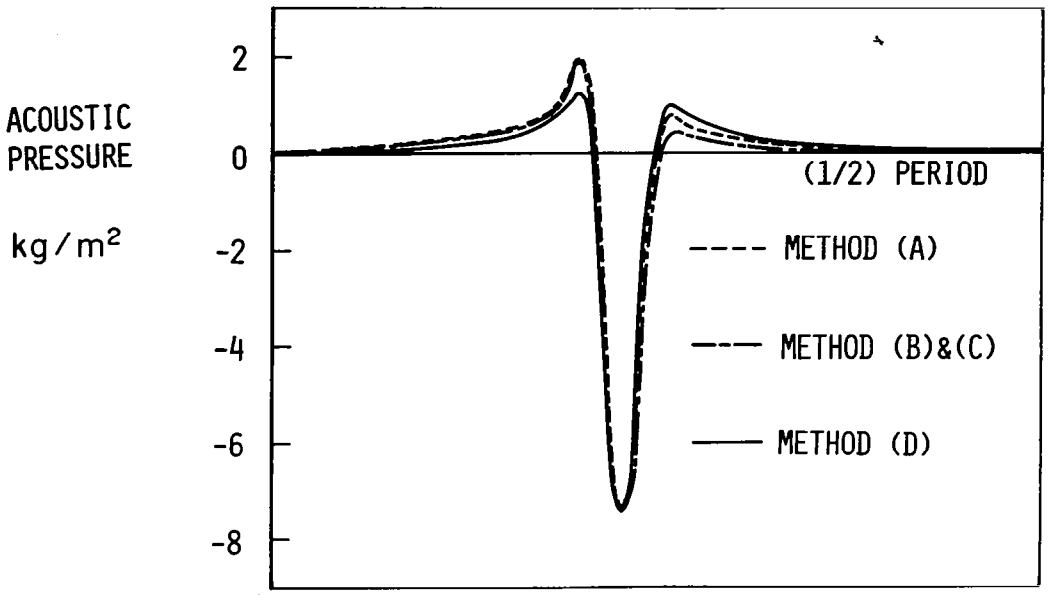

Figure 7.- Waveforms given by four methods.

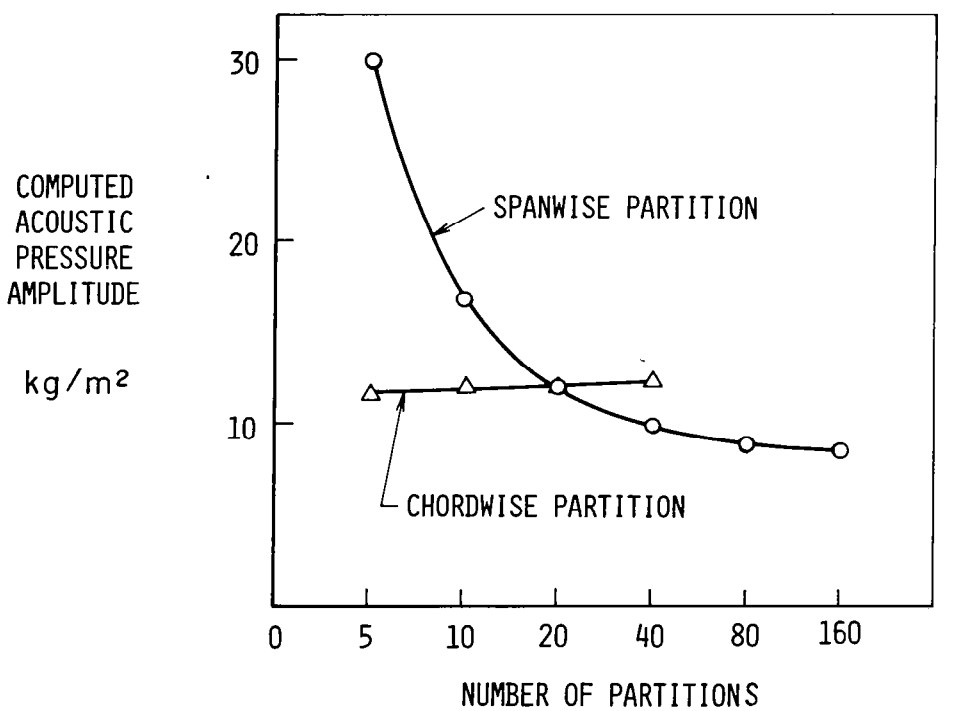

Figure 8.- Converging tendency with the number of partitions.

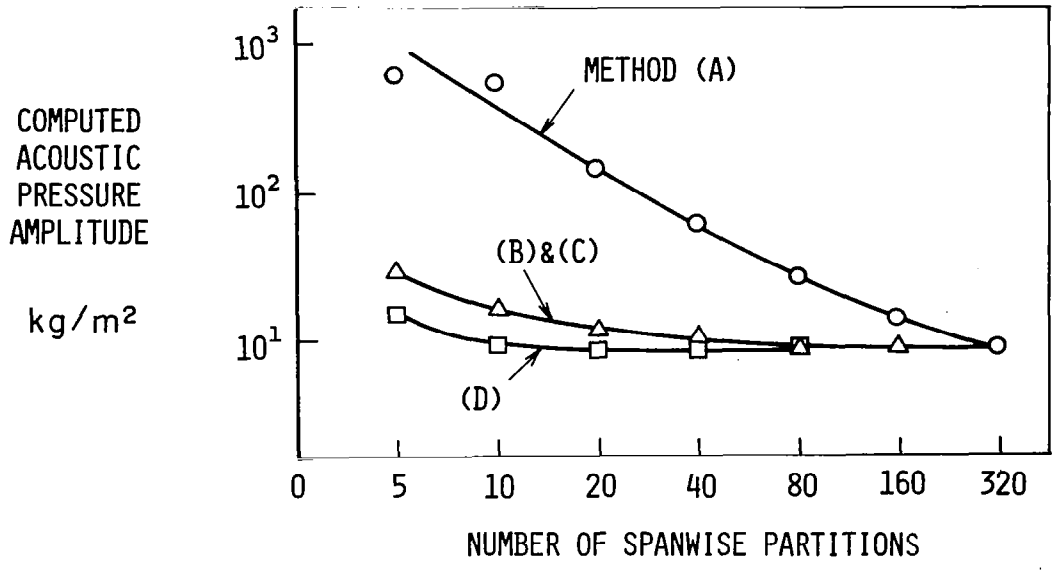

Figure 9.- Converging tendency of the four methods.

t_1 : TIME SAVED FOR A GIVEN MESH SIZE
t_2 : " IN KEEPING SAME ACCURACY BY METHOD (B)OR(C)
t_3 : " " (D)

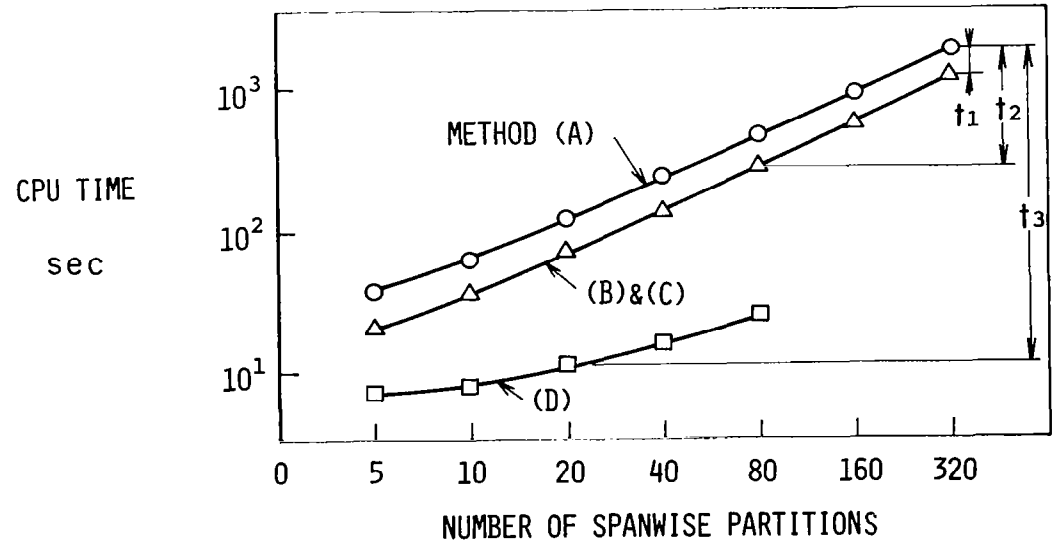

Figure 10.- A comparison of computational time between four methods.